Effects of El Niño–Southern Oscillation events on catches of Bigeye Tuna (*Thunnus obesus*) in the eastern Indian Ocean off Java

Mega L. Syamsuddin (contact author)[1,2]
Sei-Ichi Saitoh[1]
Toru Hirawake[1]
Samsul Bachri[3]
Agung B. Harto[3]

Email address for contact author: vegha16@gmail.com

[1] Laboratory of Marine Bioresource and Environment Sensing
Faculty of Fisheries Sciences
Hokkaido University
Minato-cho 3-1-1, Hakodate
Hokkaido 041-8611, Japan

[2] Faculty of Fisheries and Marine Sciences
Padjadjaran University
Jalan Raya Bandung-Sumedang KM. 21
Jatinangor, Bandung 40600, Indonesia

[3] Study Program of Geodetic and Geomatics Engineering
Faculty of Earth Sciences and Technology
Bandung Institute of Technology
Jalan Ganesha 10
Bandung 40132, Indonesia

Abstract—The effects of El Niño–Southern Oscillation events on catches of Bigeye Tuna (*Thunnus obesus*) in the eastern Indian Ocean (EIO) off Java were evaluated through the use of remotely sensed environmental data (sea-surface-height anomaly [SSHA], sea-surface temperature [SST], and chlorophyll-*a* concentration), and Bigeye Tuna catch data. Analyses were conducted for the period of 1997–2000, which included the 1997–98 El Niño and 1999–2000 La Niña events. The empirical orthogonal function (EOF) was applied to examine oceanographic parameters quantitatively. The relationship of those parameters to variations in catch distribution of Bigeye Tuna was explored with a generalized additive model (GAM). The mean hook rate was 0.67 during El Niño and 0.44 during La Niña, and catches were high where SSHA ranged from –21 to 5 cm, SST ranged from 24°C to 27.5°C, and chlorophyll-*a* concentrations ranged from 0.04 to 0.16 mg m^{-3}. The EOF analysis confirmed that the 1997–98 El Niño affected oceanographic conditions in the EIO off Java. The GAM results indicated that SST was better than the other environmental factors (SSHA and chlorophyll-*a* concentration) as an oceanographic predictor of Bigeye Tuna catches in the region. According to the GAM predictions, the highest probabilities (70–80%) for Bigeye Tuna catch in 1997–2000 occurred during oceanographic conditions during the 1997–98 El Niño event.

Manuscript submitted 4 June 2012.
Manuscript accepted 1 March 2013.
Fish. Bull 111:175–188 (2013)
doi 10.7755/FB.111.2.5

The El Niño–Southern Oscillation (ENSO) is a large-scale pattern of climate fluctuation that strongly influences much of the globe. In the Pacific, the ENSO cycle causes warm phases (El Niño) and cool phases (La Niña) that have been shown to affect catches in tuna fisheries (Lehodey et al., 1997; Lehodey, 2001). The approximate onset of the 1997–98 El Niño event occurred during March–April 1997, and the mature phase in November–December 1997 (Enfield, 2001). The El Niño event ended in May 1998 and a cold La Niña was established in the eastern Pacific. The 1997–98 El Niño was the strongest on record and affected the climate in many parts of the world (McPhaden, 1999). Catches of tunas around the world are affected by ENSO events (Howell and Kobayashi, 2006; Lehodey et al., 2010). Therefore, for sustainable management of Bigeye Tuna (*Thunnus obesus*) resources in the eastern Indian Ocean (EIO) off Java, one of the main islands in Indonesia, understanding the effects of ocean climate variability on catch distribution is essential.

The Bigeye Tuna is a productive tropical species that accounts for more than 10% of the total catch of market tuna species worldwide (Miyake et al., 2010). Bigeye Tuna is a commercially targeted species and represents one of the most valuable species of longline fisheries in the EIO off Java (ISSF[1]). It is a highly migratory species that is distributed between 40°N and 40°S in all 3 major oceans, except in the southwestern sector of the Atlantic (Hanamoto, 1987). Bigeye Tuna generally favor water temperatures between 17°C and 22°C. They prefer to stay near, and usually below, the

[1] ISSF (International Seafood Sustainability Foundation). 2012. ISSF stock status ratings—2012: status of the world fisheries for tuna. ISSF Tech. Rep. 2012-04, 88 p. [Available from http://iss-foundation.org/resources/downloads/?did=328, accessed November 2012.]

thermocline and come to the surface periodically (Pepperell, 2010). The main depth range of fishing for Bigeye Tuna in the Indian Ocean is 161–280 m (Mohri and Nishida, 1999), although they can inhabit the depth range of 0–100 m during the night (Howell et al., 2010).

Sea-surface-height can be used to infer oceanic features such as current dynamics, fronts, eddies, and convergences (Polovina and Howell, 2005), and sea-surface temperature (SST) has been used to investigate productive frontal zones (Zainnudin et al., 2004), both of which can be used to indicate potential tuna fishing grounds. Thermal (or color) gradients in satellite images that arise from the circulation of water masses often indicate areas of high productivity (Saitoh et al., 2009). Chlorophyll-*a* data can also be used as a valuable indicator of water mass boundaries and may identify upwelling that can influence tuna distribution in a region.

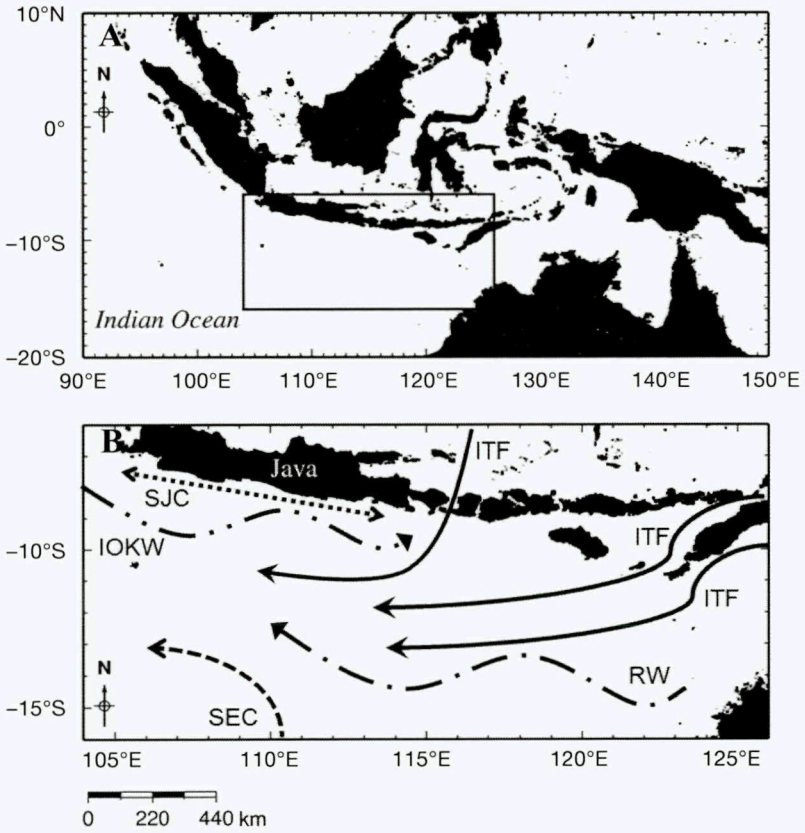

Figure 1

(**A**) Map of the Indonesian seas, with the inset box representing the study area. (**B**) Map of the study area in the eastern Indian Ocean (EIO) off Java for our analyses of how El Niño–Southern Oscillation events may affect catch rates of Bigeye Tuna (*Thunnus obesus*). In panel B, the wave and current systems in the EIO off Java are indicated by the dotted line for the South Java Current (SJC), solid lines for the Indonesian Throughflow (ITF), the line with dashes and 2 dots for the Indian Ocean Kelvin Waves (IOKWs), the line with dashes and 1 dot for the Rossby Waves (RWs), and the dashed line for the Indian Ocean South Equatorial Current (SEC).

The effects of ENSO on oceanographic conditions and tuna catches in the Pacific have been reported widely (Lehodey et al., 1997; Torres-Orozco et al., 2006; Briand et al., 2011). High catch rates of Albacore (*Thunnus alalunga*) in the southwest Pacific Ocean were found to correspond with high negative Southern Oscillation Index values during strong El Niño events (Briand et al., 2011). The effects of ENSO events on Bigeye Tuna catches have been well studied in the western Pacific Ocean (Miller, 2007) but less studied in the Indian Ocean. Most Indian Ocean studies have focused on the relationship between oceanographic parameters and the distribution of Bigeye Tuna (Mohri and Nishida, 1999; Song et al., 2009, Song and Zhou, 2010), the correlation of a single oceanographic factor with ENSO (Yoder and Kennely, 2003), or oceanographic variability in the interior Indonesian seas (Zhou et al., 2008; Sprintall et al., 2009).

Here, we focus on the ways in which climate variability affects oceanographic conditions and catch rates of Bigeye Tuna in the EIO off Java. To obtain a more detailed description of the spatiotemporal characteristics of those oceanographic parameters, we applied the empirical orthogonal function (EOF). Further analysis was undertaken with a generalized additive model (GAM) to examine the relationship between oceanographic conditions and catch rates of Bigeye Tuna. The ultimate goal of this study was to understand how catch rates of Bigeye Tuna in the EIO off Java are affected by ENSO events.

Materials and methods

Study area

The study area was located in the EIO, south of Java, spanning between 6–16°S and 104–126°E (Fig. 1B). This area has complex dynamic currents and wave systems. The dominant current and wave features include 1) the Indonesian Throughflow (ITF), outflow water from the Pacific to the Indian Ocean (Molcard et al., 2001; Gordon et al., 2010); 2) the seasonally reversing South Java Current (SJC) along the southern coast of the Indonesian Sea (Sprintall et al., 2010); 3) the Indian Ocean South Equatorial Current (SEC) that flows from the southern Indian Ocean to an area off southern Java (Zhou et al., 2008); 4) downwelling Indian Ocean Kelvin Waves (IOKWs) that propagate to the east along the coasts of west Sumatra, Java, and the lesser Sunda islands (Syamsudin et al.,

2004); and 5) westward Rossby Waves propagation at 12–15°S (Gordon, 2005; Sprintall et al., 2009).

Besides these current and wave systems, winds over the Indonesian maritime continent and the position of the Intertropical Convergence Zone are dominant features of strong monsoon signatures. During the southeast monsoon (May to October), southeasterly winds from Australia generate upwelling along the southern coasts of Java and Bali. These conditions are reversed during the northwest monsoon (November to April) (Gordon, 2005).

Data

For our study, we used fishery catch data and satellite remotely sensed data. Bigeye Tuna catch data and remotely sensed environmental data for the period of 1997–2000 were analyzed. These data included the ENSO components of an El Niño event (April 1997–May 1998) and a La Niña event (July 1998–June 2000).

Fisheries data sets Catch data for Bigeye Tuna were obtained from longline fishing logbooks provided by PT Perikanan Nusantara,[2] an incorporated company of the Indonesian government, at Benoa, Bali. Data included fishing position (latitude and longitude), operational days, fish weight (in kilograms), vessel number, number of hooks, and the number of fish caught per month during 1997–2000. The fishing locations recorded in the logbook were only the fishing positions where Bigeye Tuna were caught (there were no data for the locations where no fish were caught). These data were compiled into grids of 1° latitude×1° longitude because catch data for Bigeye Tuna were available only at a resolution of 1°. From this data set, the catch rate of Bigeye Tuna was expressed as a percentage of hook rate (HR). The HR was calculated as the number of fish caught (individuals/month) per 100 hooks. The HR, therefore, shows how many tuna were hooked per unit of 100 longline hooks, and the HR can be referred to as catch per unit of effort.

The majority of fishing operations were conducted by medium-size vessels (100 gross tonnage). The number of vessels in operation was 19–20 per month, and vessels used the same fishing gear (longline sets) and similar fishing techniques. The number of fishing sets was within the range of 910–1607 per year. The longline sets were specifically designed and constructed to reach the swimming depths of the Bigeye Tuna. PT Perikanan Nusantara[3] used 2 types of longline sets constrained by the fishing depth during operation: 1) a shallow set (depth <100 m; consisting of 4–6 branch lines between floats) and 2) a deep set (depth 100–300 m; consisting of 10–14 branch lines between floats). The deep set was used to catch Bigeye Tuna, and the shallow set was better suited to catchYellowfin Tuna (*Thunnus albacares*). The longline fishery targeted Bigeye Tuna at operational depths of 109–288 m during night sets. Each deep set consisted of 10–14 branch lines between floats and 800–1600 hooks per set. The fishing ground covered an area located around 10–16°S and 108–120°E; fishing operations were limited to 15 days per trip because of fuel costs and the need to keep caught fish fresh (Perikanan Nusantara[3]).

Bigeye and Yellowfin Tunas were distinguished by various characteristics, including the following features: the Bigeye Tuna is longer, has a large head, large eyes, a dusky-colored tail, yellowish finlets edged in black, and a tail with a flat, trailing edge. The Yellowfin Tuna is shorter, has a smaller head, round and small eyes, a narrow body, a yellowish tail, and a notch in the center of its tail (Itano[4]).

Remotely sensed data Remotely derived environmental variables included the sea-surface-height anomaly (SSHA), SST, and chlorophyll-*a* concentration. The SSHA data with a spatial resolution of 1/3°, derived from the TOPEX/Poseidon and ERS-1/2 altimeter measurements, were produced and distributed by Archiving, Validation and Interpretation of Satellite Oceanographic Data (AVISO, http://www.aviso.oceanobs.com). We obtained 7-day composite cycles of SSHA products to calculate the monthly mean SSHA. SST data were derived from the Advanced Very High Resolution Radiometer sensor on board NOAA satellites. This data set is distributed by the Physical Oceanography Distributed Active Archive Center (http://podaac.jpl.nasa.gov) of the Jet Propulsion Laboratory of the National Aeronautics and Space Administration (NASA). We used the monthly mean SST data set at a pixel resolution of 4×4 km. Chlorophyll-*a* data were derived from images obtained from the

Sea-viewing Wide Field-of-view Sensor (SeaWiFS) Project (level 3) and were of a spatial resolution of 9×9 km for the period from September 1997 to December 2000 (monthly composite data were downloaded from http://oceancolor.gsfc.nasa.gov). These data were processed with the SeaWiFS Data Analysis System virtual appliance (SeaDAS VA, vers. 6.1) of NASA (http://seadas.gsfc.nasa.gov/seadasva.html).

SSHA and SST images were matched with the 9-km-resolution spatial scale for chlorophyll-*a* concentrations. The 9-km-resolution data were used to capture dynamic features of the oceanographic conditions that represented El Niño and La Niña events and to show spatial patterns for the EOF analysis. However, for the

[2] Mention of trade names or commercial companies is for identification purposes only and does not imply endorsement by the National Marine Fisheries Service, NOAA.

[3] Perikanan Nusantara, Inc. 2001. Vessels operation data of Incorporated Company of Perikanan Nusantara, 78 p. Perikanan Nusantara, Jakarta, Indonesia.

[4] Itano, D. G. 2005. A handbook for identification of yellowfin tuna and bigeye tuna in fresh condition, vers. 2, 27 p. Pelagic Fisheries Research Program, Univ. Hawaii, Honolulu. [Available from ftp://ftp.soest.hawaii.edu/PFRP/itano/1_BE-YF%20ID%20Fresh_ENGLISH_v2_logo.pdf, accessed November 2012.]

GAM input, SSHA, SST, and chlorophyll-*a* data were calculated on a spatial grid of 1°×1° to match with the spatial resolution of the fisheries data. We resampled the remotely sensed data to resolutions of 9 km and 1° through the use of geographic information system tools, including Generic Mapping Tools (GMT, vers. 4.5.7 [Wessel and Smith, 1998]), with the nearest-neighbor technique. Nearest-neighbor assignment can be applied with the resample function as a preprocessing step before combination of raster data of different resolutions. This assignment does not change any of the values of cells from the input raster data sets; the cell center from the input raster that is closest to the cell center for the output processing is used.

Niño 3.4 index The Niño 3.4 index was used as a climatic index of ENSO indicators based on SST. The index is the average SST anomaly in the region bounded by 5°N to 5°S and 120–170°W. The Niño 3.4 index was downloaded from the NOAA Climate Prediction Center (http://www.cpc.ncep.noaa.gov). El Niño and La Niña events were identified if the 5-month running average of the Niño 3.4 index exceeded +0.5°C for El Niño or –0.5°C for La Niña for at least 5 consecutive months (this index is shown as the dashed line in Fig. 2A).

Catchability coefficient

Catchability was defined as the proportion of available fish in the population that would be caught by a unit of fishing effort. Catchability depends on the distribution of fishing effort in relation to the distribution of the target species (Ellis and Wang, 2007). The catchability coefficient is defined as the proportion of the total stock taken by one unit of effort (Haddon, 2011) and is expressed as

$$C / (q\ E) = B, \quad (1)$$

where C = catch;
q = the catchability coefficient;
E = the amount of fishing effort; and
B = stock biomass.

The unit of effort used for calculation of longline catch rates is the number of hooks, as a result of changes in gear practices (Ward and Meyers, 2004). We computed the catchability coefficient for all months during 1997–2000.

Empirical orthogonal function

We applied the EOF as a statistical method to quantitatively examine oceanographic parameters. EOF analysis is a useful technique for decomposition of a time series of geophysical data into temporal and spatial variability in terms of orthogonal functions or statistical modes. EOF analysis has been used commonly to describe spatiotemporal ocean variability (Yoder and Kennely, 2003; Otero and Siegel, 2004; Radiarta and Saitoh, 2008; Tolan and Fisher, 2009).

EOF analysis was applied to the raw weekly data set of SSHA and SST and monthly data of chlorophyll-*a* concentrations because of a lack of data in many of the weekly images. Here, we examined only the first and second dominant modes, which were statistically independent and significant. A more comprehensive explanation of the concept of EOF analysis has been provided by Bjornsson and Venegas (1997). We constructed the EOF analysis using Matlab, vers. 7.1, software (The MathWorks, Inc., Natick, MA). On the basis of the results of the EOF, we generated maps of patterns of spatial and temporal ocean variability in the EIO off Java with ArcGIS tools (Esri, Redlands, CA).

Generalized additive model

The GAM was first proposed by Hastie and Tibshirani (1990). The advantage of this model is that the predictor variables have nonlinear effects upon the response variable. We applied the binomial GAM to analyze positive catches, interpreted as presence (1), and null catches, interpreted as absence (0) (Fraile et al., 2010), of Bigeye Tuna and to determine the catch probability of Bigeye Tuna in the EIO off Java. The Bigeye Tuna catch data presented here are based only on the grids fished because, as mentioned previously, catch information for Bigeye Tuna was not available for unfished grids; therefore, we ignored the unfished strata (Walters, 2003). Some sampling bias may have affected our results regarding catch variability. However, the catch data are nevertheless useful for examination of Bigeye Tuna variability in the study area, and the HR data based on those catch data may be indicative of relative changes in availability. We analyzed the presence of Bigeye Tuna through exploration of the spatial trends in their catch distribution that were influenced by SSHA, SST, and chlorophyll-*a* concentrations. All explanatory model terms were treated as continuous variables and the spline smoothers were fitted initially to each term in the model (Zuur et al., 2009). A stepwise GAM was performed to determine the best-fitting model before application of the final GAM to the entire data set. Akaike's information criteria (AIC) were used to determine the optimal set of explanatory variables. The model with the smallest AIC can be selected as the optimal model. GAMs were constructed in R software (vers. 2.14.0; R Development Core Team, 2011) with the gam function of the mgcv package (Wood, 2006). The GAMs were fitted in the form

$$g(u_i) = \alpha_0 + s_1(x_{1i}) + s2(x_{2i}) + s3(x_{3i}) + s_n(x_{ni}), \quad (2)$$

where g = the link function;
u_i = the expected value of the dependent variable (Bigeye Tuna catch);
α_0 = the model constant; and

s_n = a smoothing function for each of the model covariates x_n.

The constructed GAM could then be used to predict the Bigeye Tuna catch probability with the predict.gam function in the mgcv package in R (Wood, 2006). The Bigeye Tuna catch probability is the relative probability of catching one or more Bigeye Tuna at a location given the oceanographic conditions in the area (Teo and Block, 2010). The prediction maps were produced with the best model selected from a set of 7 models. The distribution of the GAM-predictions of Bigeye Tuna catch was compared with monthly fishery data. With GMT tools, we made monthly predictions of Bigeye Tuna catch probabilities.

Results

Catch rates of Bigeye Tuna

During the El Niño event in 1997–98, catch rates of Bigeye Tuna peaked in May–July 1997 (0.87–0.94 HR) and were still high in February–July 1998 (0.69–0.90 HR), followed by a continuous decline in the later months of 1998 (Fig. 2A). During the La Niña event in 1999–2000, catch rates were reduced throughout the year (HR <0.67). The average HR was higher during the 1997–98 El Niño event (0.67) than during the 1999–2000 La Niña event (0.44).

The number of hooks deployed ranged from 14,392 to 178,109 per month (Fig. 2B), and more hooks were used during the 1997–98 El Niño event (147,676 hooks) than during the 1999–2000 La Niña event (144,283 hooks). In June 1997, 178, 109 hooks (maximum number) were deployed and in November 2000, 14,392 hooks (minimum number) were deployed. The catchability coefficient (q) varied with the number of hooks (Fig. 2B). Catchability was high in May 1997 (1.56×10^{-7}), June 1998 (1.47×10^{-7}), and November 2000 (2.73×10^{-7}).

Catch rates of Bigeye Tuna showed seasonal variations and were higher during the southeast monsoon (May–October; SE) than during the north-

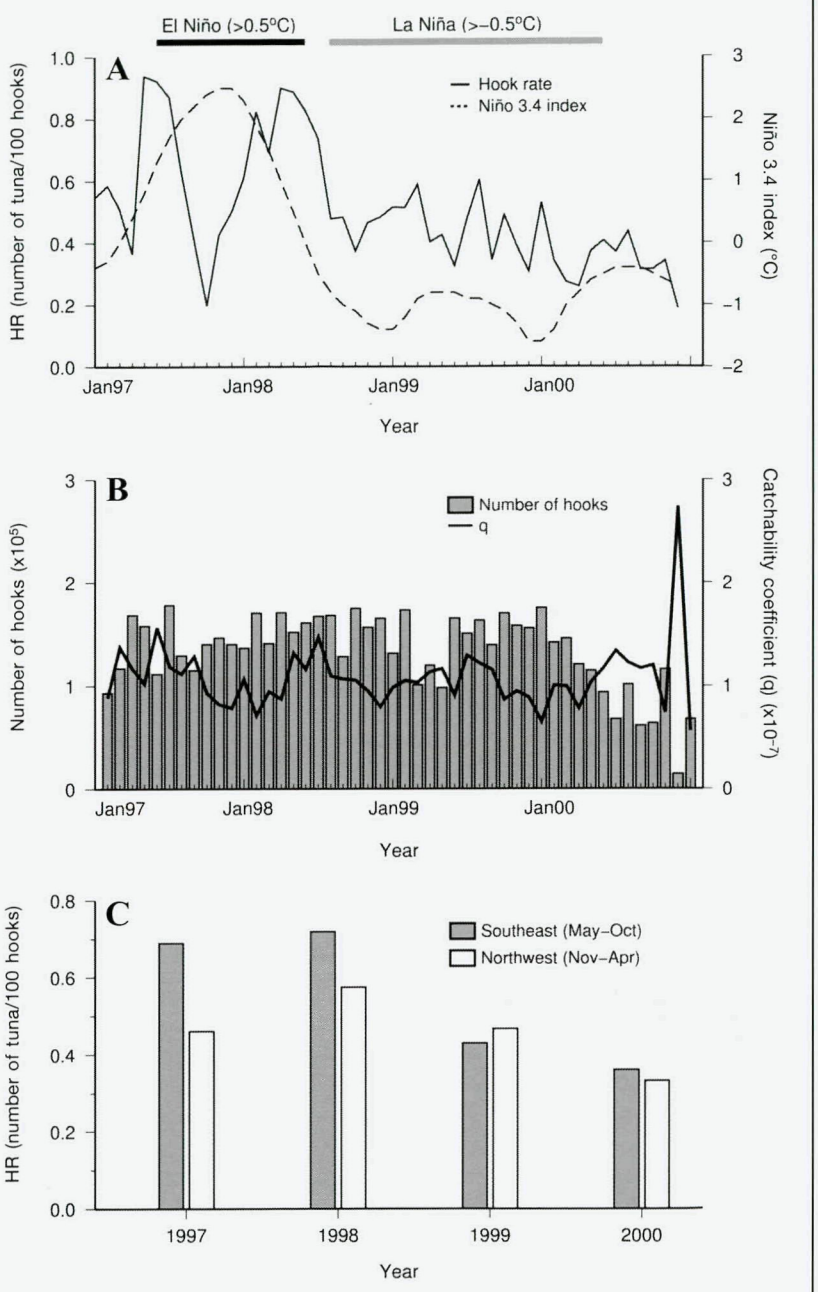

Figure 2

(**A**) Variability in catch rates of Bigeye Tuna (*Thunnus obesus*) in the eastern Indian Ocean off Java by hook rate (HR) percentage (solid line) and SST anomalies from the Niño 3.4 index during 1997–2000 (dashed line). El Niño and La Niña events were identified when the average of the Niño 3.4 index exceeded +0.5°C for El Niño or –0.5°C for La Niña for at least 5 consecutive months. The El Niño event is indicated by a black bar on the top of this graph, and the La Niña event is indicated by a gray bar on the top. (**B**) The total number of hooks deployed (gray bars) and time series variation of the catchabillity coefficient (solid line) during 1997–2000. (**C**) Seasonal variations in Bigeye Tuna HR in 1997–2000. The gray bar represents the southeast monsoon (May–October), and the white bar represents the northwest monsoon (November–April).

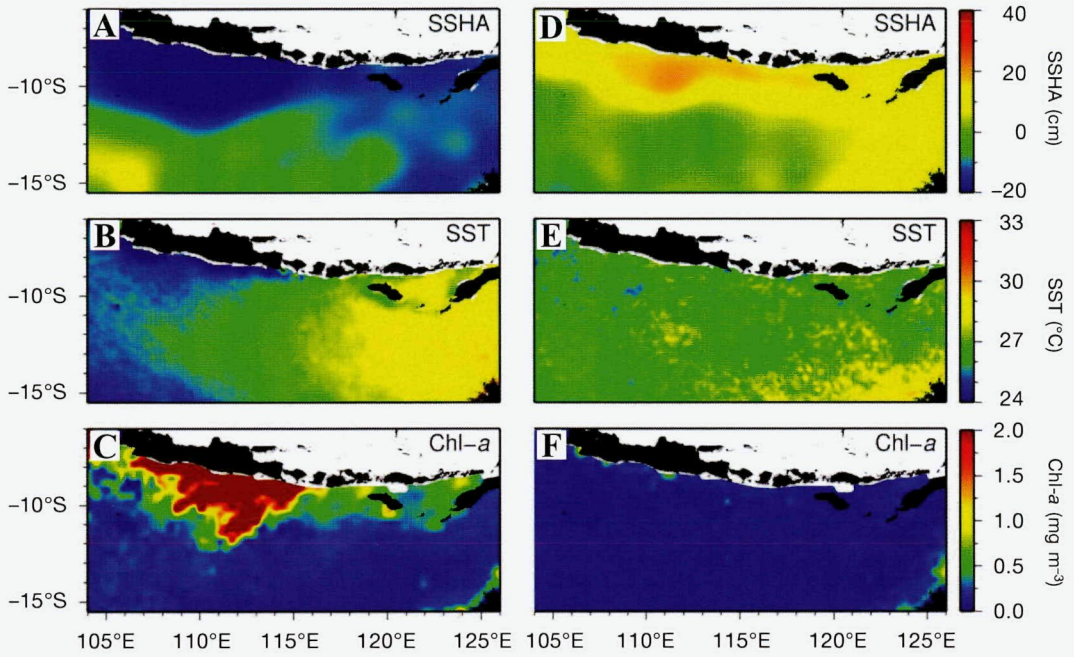

Figure 3

On the left, images of mean values for 3 months obtained from remotely sensed data of the eastern Indian Ocean off Java during El Niño event (September, October, and November 1997) for 3 parameters—(**A**) sea-surface-height anomaly (SSHA), (**B**) sea-surface temperature (SST), and (**C**) chlorophyll-*a* (chl-*a*) concentration. On the right, images of mean values for 3 months obtained during La Niña event (February, March, and April 1999) for the same 3 parameters: (**D**) SSHA, (**E**) SST, and (**F**) chl-*a* concentrations. Scale units are in centimeters, degrees Celcius, and milligrams per cubic meter for SSHA, SST, and chl-*a* data, respectively.

west monsoon (November–April; NW) for all years except 1999 (Fig. 2C). High HRs (average 0.55 HR) were recorded during the southeast monsoon, and lower HR (average 0.45 HR) occurred during the northwest monsoon.

Features of oceanographic conditions

The following results are presented to show how the different phases of ENSO affected oceanographic conditions in the EIO off Java. Figure 3 shows 6 snapshots of SSHA, SST, and chlorophyll-*a* conditions, each showing the means of values from 3 different months during different phases of El Niño (mean of September, October, and November 1997) and La Niña (mean of February, March, and April 1999) in the EIO off Java. The months that represent the El Niño and La Niña events were chosen on the basis of the 3 consecutive months with the highest individual values in the Niño 3.4 index during El Niño and La Niña during 1997–2000. There were contrasting conditions of SSHA and SST along the coasts and in offshore areas during the El Niño and La Niña events.

During the El Niño event, SSHA showed negative values (from –1 to –20 cm) along coastal regions of the EIO off Java (Fig. 3A). In contrast, offshore regions influenced by frontal areas between 10–12°S and 15°S exhibited positive SSHA (4 cm). Lower SST (24–27°C) occurred in the coastal to offshore regions of the EIO off Java (Fig. 3B), and warmer waters (29°C) appeared in the eastern part of the EIO off Java. Conversely, during the La Niña event, positive SSHA (1–13 cm) occurred along the coasts, and negative SSHA (–5 to –3 cm) were found offshore between 12° and 16°S (Fig. 3D). SST during the La Niña event both near the coasts and in offshore areas of the EIO off Java (27–29°C) were higher than values during the El Niño event in this region (Fig. 3E).

Chlorophyll-*a* concentrations were higher during the El Niño event (0.2–2.0 mg m^{-3}; mean of September, October, and November 1997; Fig. 3C) than they were during the La Niña event (0.05–0.10 mg m^{-3}; mean of February, March, and April 1999; Fig. 3F). The highest concentration of 2 mg m^{-3} was detected during the El Niño event along the coast of the EIO off Java, and values decreased toward offshore (0.01–0.20 mg m^{-3}) around the frontal area at 10–12°S (Fig. 3C). This variation in chlorophyll-*a* values coincides well with the occurrence of lower SST in the same areas during the El Niño event (Fig. 3B).

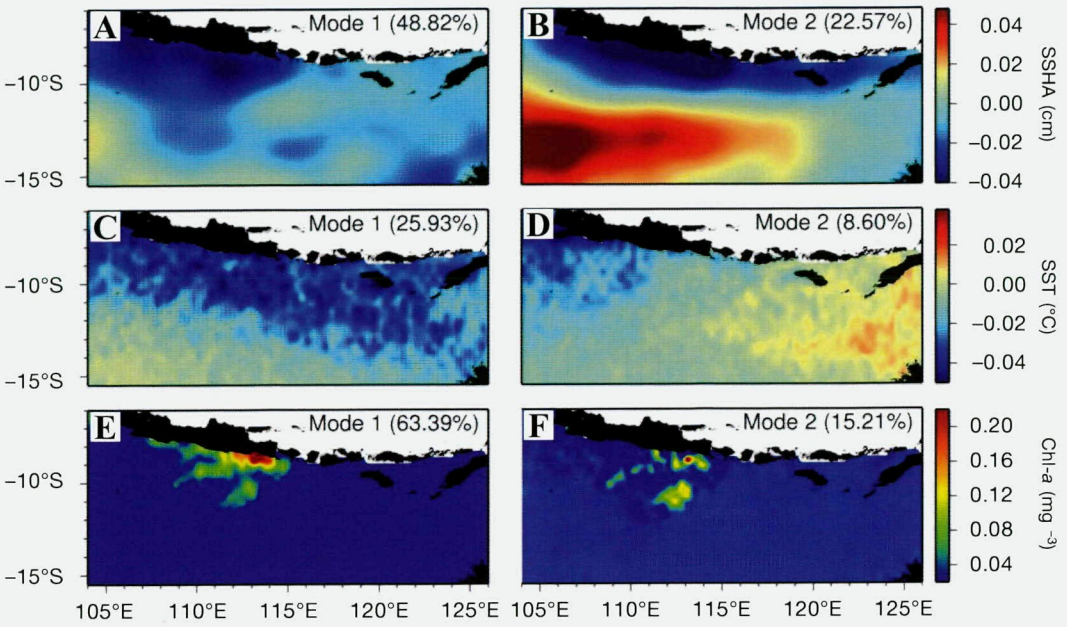

Figure 4

Spatial patterns of the empirical orthogonal function modes in the eastern Indian Ocean off Java from September 1997 to December 2000: (**A**) first mode of sea-surface-height anomaly (SSHA), (**B**) second mode of SSHA, (**C**) first mode of sea-surface temperature (SST), (**D**) second mode of SST, (**E**) first mode of chlorophyll-*a* (chl-*a*) concentrations, and (**F**) second mode of chl-*a* concentrations. Scale units are in centimeters, degrees Celcius, and milligrams per cubic meter for SSHA, SST, and chl-*a* data, respectively.

Spatial and temporal modes of ocean variability

The remote forcing in the timescale of interannual and seasonal variations due to ENSO and monsoons are represented by the first and second EOF modes of SSHA, SST, and chlorophyll-*a* concentrations, with the total energy variance from these 2 modes about 78.60% for chlorophyll-*a* values, 71.39% for SSHA, and 34.53% for SST (Table 1). The first spatial mode of SSHA contributed 48.82% of the total variance, indicating waters with relatively low temperatures and with negative SSHA concentrated along the southern coast of Java (Fig. 4A). The second spatial mode of SSHA contributed 22.57% of the total variance and showed that waters with relatively low temperatures were distributed along the southern coast of the Indonesian archipelago (Fig. 4B). The first spatial mode of SSHA corresponded with interannual variability, as shown by the first temporal mode (Fig. 5A). A map of the second spatial mode of SSHA clearly shows that this mode corresponded with seasonal variability, as indicated by the second temporal mode (Fig. 5B).

The SSHA results were associated with the first and second spatial modes of SST, with total variances of 25.93% and 8.60%, respectively. The first spatial mode of SST showed that waters with relatively low temperatures were concentrated along the southern coast of Java, extending to the offshore area (7–13°S) (Fig. 4C). The second spatial mode of SST showed that those waters were spread along the western coast of Java (7–12°S), while waters with relatively high temperatures covered the eastern part of the EIO off Java (Fig. 4D). The amplitude function of the first mode of SST corresponded with interannual variability (Fig. 5C), and the second mode corresponded with the seasonal cycle in which the maximum and minimum SST occurred during the northwest monsoon (November–April) and southeast monsoon (May–October), respectively (Fig. 5D).

Table 1

Summary of the amplitude function (percentage of the total variability) of the first and second empirical orthogonal function modes of the sea-surface-height anomaly (SSHA), sea-surface temperature (SST), and chlorophyll-*a* (chl-*a*) concentrations in the eastern Indian Ocean off Java from September 1997 to December 2000.

Parameter	Mode 1 (%)	Mode 2 (%)	Total modes 1 and 2 (%)
SSHA	48.82	22.57	71.39
SST	25.93	8.60	34.53
Chl-*a*	63.39	15.21	78.60

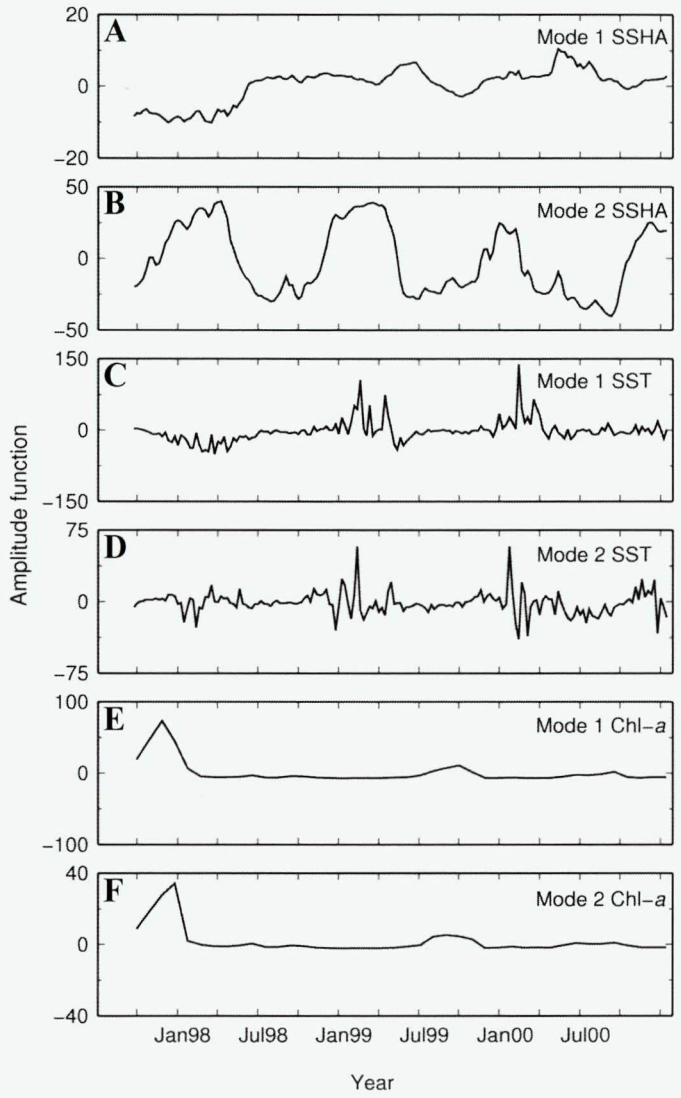

Figure 5

Amplitude function from the temporal mode of the analysis for the study area in the eastern Indian Ocean off Java from September 1997 to December 2000: (**A**) first mode of sea-surface-height anomaly (SSHA) (interannual signal), (**B**) second mode of SSHA (seasonal signal), (**C**) first mode of sea-surface temperature (SST) (interannual signal), (**D**) second mode of SST (seasonal signal), (**E**) first mode of chlorophyll-*a* (chl-*a*) concentrations (interannual signal), and (**F**) second mode of chl-*a* concentrations (annual signal). The *x*-axis represents the year, and the *y*-axis shows the amplitude function for each mode (nondimensional).

The first EOF mode of SSHA and SST showed an inverse relationship with the first EOF mode of chlorophyll-*a*, with a negative SSHA value and relatively low SST followed by higher chlorophyll-*a* concentrations along the southern coast of Java. The first mode of chlorophyll-*a* contained 63.39% of the energy variance, and the second mode contributed 15.21% of the energy variance, with notably higher chlorophyll-*a* levels concentrated along the southern coast of Java (7–9°S). The amplitude function of the first mode of chlorophyll-*a* corresponded with interannual variability, and the second mode corresponded with the annual cycle. Positive values (chlorophyll-*a* concentrations greatly elevated above values seen in other periods) occurred during September–November 1997 (Fig. 5, E–F).

Generalized additive models

The results of the GAMs are presented as 1-parameter, 2-parameter, and 3-parameter models (Table 2). All of the variables used were statistically highly significant ($P<0.0001$) for SSHA, SST, and chlorophyll-*a* concentrations. The addition of predictor variables at different levels resulted in an increase in the deviance in catch rates explained. In the 1-parameter models, SST explained the highest deviance (6.48%) and chlorophyll-*a* concentrations explained the lowest deviance (2.04%). The 3-parameter combination models explained the highest deviance (16.30%) and had the lowest AIC values.

GAM plots can be interpreted as the individual effects of predictor variables associated with SSHA, SST, and chlorophyll-*a* concentrations on Bigeye Tuna catch (Fig. 6, A–C). High probabilities of Bigeye Tuna presence were observed for SSHA ranging from –21 to 5 cm, for SST ranging from 24° to 27.5°C, and for chlorophyll-*a* levels ranging from 0.04 to 0.16 mg m^{-3}. Negative effects on Bigeye Tuna were observed for SSHA >5 cm, SST values >27.5°C, and chlorophyll-*a* values of 0.01–0.03 mg m^{-3} and >0.16 mg m^{-3}.

Spatial predictions for catch distribution of Bigeye Tuna were compared with the actual monthly fishery data collected during the El Niño (September and October 1997) and La Niña (March and April 1999) events. The predicted catch distribution of Bigeye Tuna in September 1997 during the El Niño event indicated a potential area with higher catch probability of approximately 70–80% at 10–16°S and 104–122°E, and the actual Bigeye Tuna fishing locations (with a HR of 0.41) occurred in the area between 12–16°S and 110–115°E (Fig. 7A). In October 1997, spatial predictions for catch distribution of Bigeye Tuna indicated locations with higher catch probability (60–70%) in the west at 7–12°S, 104–108°E and 14–16°S, 109–114°E, but the actual Bigeye Tuna fishing locations were located at 12–15°S, 110–116°E, where there was a predicted catch probability of around 20–40% and actual HR of only 0.20 (Fig. 7B). The

Table 2

Results from general additive models (GAMs) derived from catch rates of Bigeye Tuna (*Thunnus obesus*) in the eastern Indian Ocean off Java in 1997–2000 as a function of the oceanographic parameters (N=2843 samples). The best model was selected on the basis of the significance of predictor terms, reduction of Akaike's information criterion (AIC), and increase in cumulative deviance explained (CDE). SST=sea-surface temperature; SSHA=sea-surface-height anomaly; chl-*a*=chlorophyll-*a* concentrations estimated from SeaWiFS level-3 images (http://oceancolor.gsfc.nasa.gov).

Model		Variable	P value	AIC	CDE (%)
SST		SST	$<2.00 \times 10^{-16}$***	2117.04	6.48
SSHA		SSHA	$<2.00 \times 10^{-16}$***	2153.88	4.95
Chl-*a*		Chl-*a*	$<2.00 \times 10^{-16}$***	2219.38	2.04
SSHA	+	SSHA	$<2.00 \times 10^{-16}$***	2110.55	7.18
chl-*a*		Chl-*a*	$<2.00 \times 10^{-16}$***		
SST	+	SST	$<2.00 \times 10^{-16}$***	2065.54	9.20
chl-*a*		Chl-*a*	$<2.00 \times 10^{-16}$***		
SSHA	+	SSHA	$<2.00 \times 10^{-16}$***	1973.96	13.30
SST		SST	$<2.00 \times 10^{-16}$***		
SSHA	+	SSHA	$<2.00 \times 10^{-16}$***	1912.79	16.30
SST	+	SST	$<2.00 \times 10^{-16}$***		
chl-*a*		Chl-*a*	$<2.00 \times 10^{-16}$***		

***indicates statistical significance at the 0.001 level.

suspected shift in the distribution of Bigeye Tuna away from the fishing grounds caused the drop in the HR from 0.41 in September 1997 to 0.20 in October 1997.

During La Niña in 1999, spatial predictions indicated Bigeye Tuna catches with lower probabilities of 20–40% occurring in the offshore area of the western part of the EIO off Java. In March 1999, the spatial prediction of Bigeye Tuna catch (20–30%) was located around 12–16°S, 104–115°E, but actual Bigeye Tuna fishing locations were at 13–15° S, 106–107° E; 12–15°S, 109–112°E; and 12–13°S, 114–115°E (Fig. 7C). The spatial prediction of Bigeye Tuna catch (20–40%) moved to the west at 11–16° S and 104–111°E in April 1999 (Fig. 7D), but the actual Bigeye Tuna catch areas were located at 13–14°S and 11–15°S in the longitude range of 108–118°E.

Discussion

Catch rates of Bigeye Tuna varied over a range of time scales and apparently in relation to environmental changes. Changes in oceanographic conditions during ENSO events resulted in perceivable variations in Bigeye Tuna catches, with an average HR of 0.67 during the 1997–98 El Niño event. The 1999–2000 La Niña event, with an average HR of 0.44, was less favorable for catches.

The spatial patterns of the first and second EOF modes for SSHA, SST, and chlorophyll-*a* concentration gave typical negative SSHA, low SST, and high chlorophyll-*a* concentration along the southern coast of the Indonesian archipelago, and changes in these patterns could be exposed by the temporal mode as interannual variation related to the forcing of the 1997–98 El Niño event and upwelling evidence. Those typical spatial patterns are consistent with the oceanographic conditions during September–November 1997 (Fig. 3, A–C). The first and second modes of chlorophyll-*a* showed the characteristics of an upwelling pattern, with chlorophyll-*a* concentrations higher along the southern coast of Java than in other areas. Although it normally ends in October, upwelling was observed into November during the southeast monsoon in the El Niño event in 1997.

Our results are consistent with the findings of Sprintall et al. (1999) and Ffield et al. (2000), who reported that the ITF brings colder and warmer waters to the Indian Ocean during El Niño and La Niña events, respectively, and the local, alongshore winds south of Java are favorable for upwelling through December. They also confirmed that the upwelling signal could account for the reduced downwelling signal from the November Kelvin waves. In November 1997, Kelvin waves were not generated in the region and this condition caused the persistence of colder water along the southern coast of Java.

Chlorophyll-*a* concentrations contributed the highest energy variance, indicating that chlorophyll-*a* concentration was the main indicator of the forcing mechanisms responsible for the 1997–98 El Niño event. Our

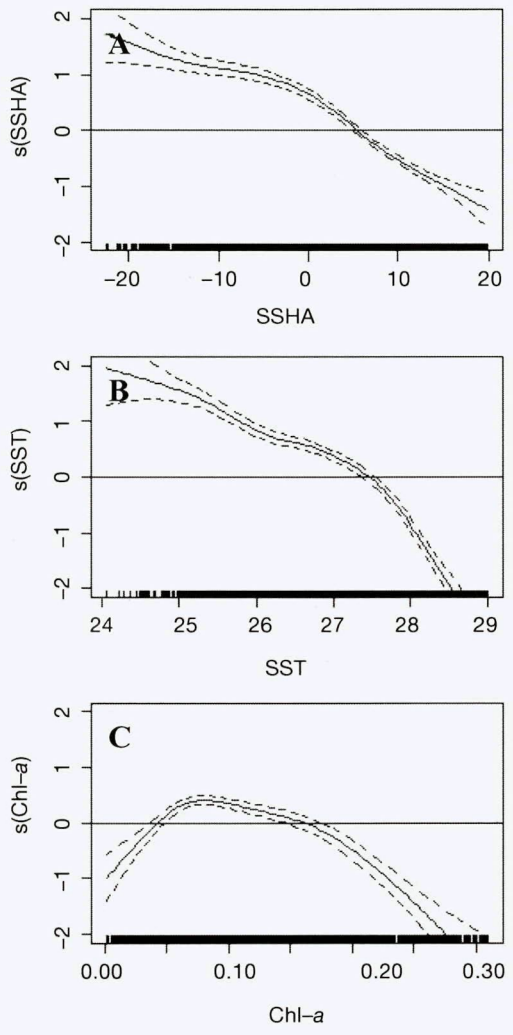

Figure 6

Effect of the 3 oceanographic variables—(**A**) sea-surface-height anomaly (SSHA), (**B**) sea-surface temperature (SST), and (**C**) chlorophyll-*a* (chl-a) concentrations—on Bigeye Tuna (*Thunnus obesus*) catches derived from generalized additive model (GAM) of presence-absence data. The *x*-axis shows the values of the explanatory variables, and the *y*-axis shows the results of smoothing the fitted values. The tick marks on the horizontal axis represent the values of the observed data points; the solid line indicates the fitted function. Dashed lines represent 95% confidence intervals. The horizontal line at zero indicates no effect. The percent frequency of occurrence was higher for all values for which the fitted GAM function was above the zero axis and lower for values <0.

results are consistent with the work of Murtugudde et al. (1999), who showed that, in the Indian Ocean, intense El Niño events, such as the one in 1997–98, have direct effects on primary production and cause anomalous high values of chlorophyll-*a* concentration observed in the EIO. Upwelling areas are potential convergence zones for plankton aggregation, attracting larger predators, such as tunas (Lehodey et al., 1997). Such concentrations of chlorophyll-*a* may cause the increased catches during El Niño event (Polovina et al., 2001; Lehodey et al., 2003; Polovina et al., 2004; Miller, 2007).

We used a binomial GAM to investigate the effects of environmental variables that affect the catchability of Bigeye Tuna. The effects of oceanographic conditions inferred from the GAM indicated that oceanographic factors strongly influence the catchability of Bigeye Tuna. SST was a more important oceanographic predictor of Bigeye Tuna catches than were the other environmental variables (SSHA and chlorophyll-*a*) in this region. Furthermore, this result from GAM analyses of SST indicates that remote forcing from the Pacific Ocean has a large effect on HR during an El Niño because of the reduction in heat transported from the Pacific to the Indian Ocean by the Indonesian Throughflow during El Niño events (Ffield et al., 2000; Gordon et al., 2010). Bigeye Tuna are very sensitive to changes in SST (Holland et al., 1992; Brill et al., 2005). Our results indicate that Bigeye Tuna catches increased in areas with relatively low temperatures (24–27.5°C) and decreased at temperatures >27.5°C (Fig. 6B). Our results are supported by previous research from the North Pacific Ocean, in which SST had the greatest effect on Bigeye Tuna at temperatures of 23–26.5°C (Howell et al., 2010).

SSHA was the second-most significant oceanographic predictor of Bigeye Tuna catch distribution in the EIO off Java. We used SSHA to understand oceanic variability, such as current dynamics, eddies, convergences, and divergences, which could be used as proxies for the potential location of tuna catches (Polovina and Howell, 2005). Our study showed that the preferred habitat for Bigeye Tuna was in the range of SSHA values of –21 to 5 cm (Fig. 6A). This finding indicates that Bigeye Tuna forage in areas of low and negative SSHA values in contrast to divergences in SSHA values. Howell and Kobayashi (2006) also found the presence of a strong gradient of sea-surface height in the region of Palmyra Atoll during the 1997–98 El Niño, coinciding with an increase in the geostrophic (subsurface) flow that may increase shoaling of longline sets. Negative SSHA would push the thermocline upward, nearer the surface, and the elevation of the thermocline would allow Bigeye Tuna from below to become more accessible to longline gear. This preferred condition may enhance the potential Bigeye Tuna habitat, as it apparently did during the 1997–98 El Niño, when increased Bigeye Tuna catches occurred. Our findings seem to agree with the results of Holland et al. (1992) and Brill (1994), who reported that Bigeye Tuna move toward cooler habitats to prevent overheating, with negative values of SSHA indicating that Bigeye Tuna are attracted only to shallow water when the thermocline is closer to the surface (Arrizabalaga et al., 2008).

Among the 3 environmental predictors assimilated in the model, chlorophyll-*a* concentrations exhibited the

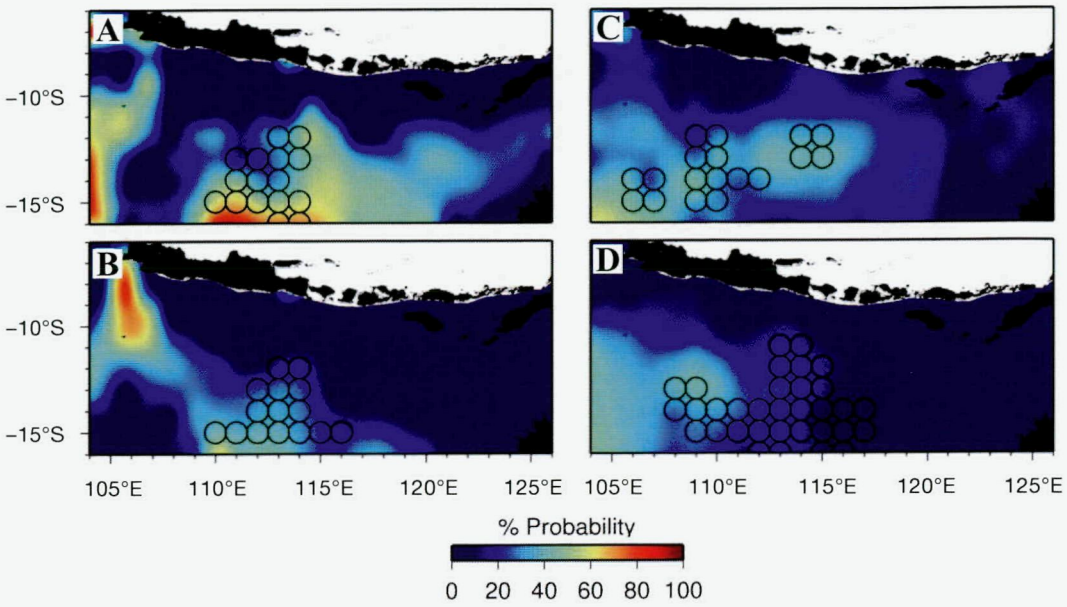

Figure 7

Spatial prediction for catch probabilities of Bigeye Tuna (*Thunnus obesus*) overlaid with actual fishing locations of Bigeye Tuna catch in the eastern Indian Ocean off Java for the El Niño event in (**A**) September 1997 and (**B**) October 1997 and for the La Niña event in (**C**) March 1999 and (**D**) April 1999. Color bars show the level of predicted catch probability of one or more Bigeye Tuna catches (0–100%); blue indicates the lowest catch probability (0), and red indicates the highest catch probability (100%). Circles outlined in black show the actual fishing locations for Bigeye Tuna catch (1° intervals). The original data set was gridded in 1° increments and smoothed for the purposes of better visualization.

lowest contribution to the model prediction. However, the derived relationship between this parameter and catches of Bigeye Tuna was statistically significant ($P<0.0001$). Bigeye Tuna fishing sets were located in waters with relatively low-to-moderate chlorophyll-*a* values. Chlorophyll-*a* data is a valuable proxy for water mass boundaries and upwelling events. Overall, the GAM results showed that the distribution of Bigeye Tuna catch in the study area was influenced primarily by SST and SSHA. The lag time in food chain processes may explain the rather weak effect of chlorophyll-*a* concentration on HR.

Bigeye Tuna catchability could be influenced by many factors, in addition to oceanographic parameters, such as the depth range of longline sets, duration of longline operations, competition among gears, number of hooks, and experience level of the fishermen (Polacheck, 1991; Ward, 2008). In this study, the fishermen used the same fishing gear with similar fishing techniques. Therefore, we assumed that differences in fishing gear did not affect the catchability of Bigeye Tuna and we considered the number of hooks and environmental conditions to explain the catchability of Bigeye Tuna. Catchability fluctuated within and between years in relation to the number of hooks. During El Niño, high catchability coefficients occurred in May 1997 (1.56×10^{-7}) and June 1998 (1.47×10^{-7}), coinciding with high HR of 0.94 and 0.83, respectively. This high coefficient number of catchability could be due to the higher number of hooks and catch of Bigeye Tuna during El Niño events related to oceanographic conditions favorable to Bigeye Tuna. The favorable oceanographic conditions were indicated by negative SSHA and by a colder SST than the normal condition of around 28–29°C. Marsac and Blanc (1999) reported that the anomalous upwelling conditions that occurred in the EIO, providing biological enrichment and a shallower thermocline, should have favored catchability in the purse-seine fishery for Bigeye Tuna during the 1997–98 El Niño. The catchability coefficient for November 2000 in our study appeared as an outlier. In that month, adverse weather conditions resulted in a decreased number of hooks and a lower HR; the increased catchability may have been due to the reduced fishing competition among longliners.

The favorable oceanographic conditions for Bigeye Tuna catches during El Niño resulted in increasing predicted catch probabilities for Bigeye Tuna. The predicted distribution of Bigeye Tuna catch during El Niño showed a potential area with higher catch probability compared with catch probability for La Niña events. Between the El Niño and La Niña events, fishing effort within the fishing grounds did not shift as much as did the predicted tuna habitat. Most catches

were made in the area of lower catch probabilities; however, some were from the boundary regions of high probability in the offshore waters of Java. Predictions of higher catch probabilities of Bigeye Tuna catches appeared to be associated with frontal areas in 10–12°S, a region that seemed to reveal the importance of the confluence on the eastward IOKW and SJC that met with the outflow of the ITF and SEC in the offshore area of the EIO off southern Java.

There were many potential fishing locations that were not used optimally, and this inefficient use reduced the total catch to much less than the level that was expected during the El Niño 1997–98 year. Nonetheless, the catch remained significantly higher during this El Niño event than during the 1999–2000 La Niña event. The mismatch between optimal fishing locations and actual fishing locations can be attributed to one or more of the reasons outlined below:

The fishermen did not have the capability to determine potential Bigeye Tuna habitats on the basis of large-scale regional shifts in oceanographic and climate regimes. They still used traditional methods, such as targeting locations similar to the ones where they had previously found Bigeye Tuna.

The cost of fuel limited how far the fishermen could travel in search of Bigeye Tuna. Their fishing ground covered the area around 10–16°S and 108–120°E, the same region used in our data analysis.

The fishermen did not target other species when fewer Bigeye Tuna were caught. They caught other species, such as small pelagic fishes (*Sardinella* sp. or *Euthynnus* sp.), only for their own consumption during fishing trips (not as main targets). Therefore, we assumed that other catches did not influence the fishing effort.

Political or management boundaries were not major problems facing this traditional fishing ground. Instead, the main constraints were the financial limits on long or distant fishing operations and the rapid fluctuations in fuel costs from week to week. The price of Bigeye Tuna depends on these factors: the location in which it is caught (fish caught farther from market are more expensive), the season (during the northwest monsoon, when fish abundance decreases, the price increases), and climate variability that affects environmental conditions (during El Niño event, fish generally are abundant and the price drops, and vice versa during La Niña event).

Conclusions

This study has shown the effects of ENSO-induced oceanographic conditions on catch rates of Bigeye Tuna in the EIO off Java. Spatiotemporal patterns in oceanographic conditions shown by the EOF, combined with the results of the GAMs, indicate that the 1997–98 El Niño event had a positive effect on catch rates of Bigeye Tuna in the EIO off Java.

The EOF modes further highlight that interannual and seasonal time scales are the main factors that affect ocean current variability in the study area. The EOF analysis also provides evidence for the effects of the 1997–98 El Niño event in the EIO off the southern coast of Java— the dominant features being negative SSHA, cold SST, and high chlorophyll-*a* concentrations. In terms of these environmental variables, the binomial GAM confirmed that SST was the major factor that influenced Bigeye Tuna catches. These results indicate that the use of a GAM with 3 predictor variables may facilitate the identification of areas with potentially high Bigeye Tuna catch in the EIO off Java.

Our results show significant effects of ENSO on Bigeye Tuna catches. For example, favorable oceanographic conditions corresponded with the El Niño event, as indicated by the EOF and GAM analyses. We did not consider depth range data for Bigeye Tuna catches. Further investigations into prediction of fishing ground locations through the use of long-term, historical time series of environmental conditions and fishing efforts—fishery data sets of greater spatial and temporal resolutions than the data sets used in ours study—are needed to better understand the effects of climate variability and fishing effort on changes in Bigeye Tuna catches in the EIO off Java.

Acknowledgments

The authors would like to thank the Directorate General of Higher Education of the Republic of Indonesia and the Japan Science Society, under the Sasagawa Scientific Research Grant, for their support in funding this research. We thank the 3 anonymous reviewers for their valuable comments. We appreciate J. R. Bower for reading and improving this article. We thank the Goddard Space Flight Center/NASA and Physical Oceanography Distributed Active Archive Center for the production of chlorophyll-*a* and SST data, AVISO for the distribution of SSHA data, and the NOAA Climate Prediction Center for the use of its Niño 3.4 index. We also thank the incorporated company of Perikanan Nusantara, Indonesia, which provided the fishery data.

Literature cited

Arrizabalaga, H., J. G. Pereira, F. Royer, B. Galuardi, N. Goni, I. Artetxe, I. Arregi, and M. Lutcavage.
2008. Bigeye tuna (*Thunnus obesus*) vertical movements in the Azores Islands determined with pop-up satellite archival tags. Fish. Oceanogr. 17:74–83.

Bjornsson, H., and S.A. Venegas.
1997. A manual for EOF and SVD analyses of climatic data. McGill Univ. C²GCR Rep. 97-1, 52 p.

Briand, K., M. Brett, and L. Patrick.
2011. A study on the variability of albacore (*Thunnus alalunga*) longline catch rates in the southwest Pacific Ocean. Fish. Oceanogr. 20:517–529.

Brill, R. W.
1994. A review of temperature and oxygen tolerance studies of tunas pertinent to fisheries oceanography, movement models and stock assessments. Fish. Oceanogr. 3:204–216.

Brill, R. W., K. A. Bigelow, M. K. Musyl, K. A. Fritsches, and E. J. Warrant.
2005. Bigeye tuna (*Thunnus obesus*) behavior and physiology and their relevance to stock assessments and fishery biology. Col. Vol. Sci. Pap. ICCAT 57(2):142–161.

Ellis, N., and Y. G. Wang.
2007. Effects of fish density distribution and effort distribution on catchability. ICES J. Mar. Sci. 64:178–191.

Enfield, D.B.
2001. Evolution and historical perspective of the 1997–1998 El Niño-Southern Oscillation event. Bull. Mar. Sci. 69:7–25.

Ffield, A., K. Vranes, A. L. Gordon, R. D. Susanto, and S. L. Garzoli.
2000. Temperature variability within Makassar Strait. Geophys. Res. Lett. 27:237–240.

Fraile, I., H. Murua, N. Goni, and A. Caballero.
2010. Effects of environmental factors on catch rates of FAD-associated yellowfin (*Thunnus albacares*) and skipjack (*Katsuwonus pelamis*) tunas in the western Indian Ocean. Indian Ocean Tuna Commission, IOTC-2010-WPTT-46, 22 p.

Gordon, A. L.
2005. Oceanography of the Indonesian seas and their throughflow. Oceanography 18(4):13–26.

Gordon, A., J. Sprintall, V. H. M. Aken, R. D. Susanto, S. Wijffels, R. Molcard, A. Ffield, W. Pranowo, and S. Wirasantosa.
2010. The Indonesian throughflow during 2004–2006 as observed by the INSTANT program. Dyn. Atmos. Oceans 50:115–128.

Haddon, M.
2011. Modelling and quatitative methods in fisheries, 2nd ed., 449 p. CRC Press, Boca Raton, FL.

Hanamoto, E.
1987. Effect of oceanographic environment on bigeye tuna distribution. Bull. Jap. Soc. Sci. Fish. Oceanogr. 3:203–216.

Hastie, T., and R. Tibshirani.
1990. Generalized additive models, 335 p. Chapman and Hall, New York.

Holland, K. N., R. W. Brill, R. K. C. Chang, J. R. Sibert, and D.A. Fournier.
1992. Physiological and behavioural thermoregulation in bigeye tuna (*Thunnus obesus*). Nature 358:410–412.

Howell, E. A., and D. R. Kobayashi.
2006. El Niño effects in the Palmyra Atoll region: oceanographic changes and bigeye tuna (*Thunnus obesus*) catch rate variability. Fish. Oceanogr. 15:477–489.

Howell, E. A., D. R. Hawn, and J. J. Polovina.
2010. Spatiotemporal variability in bigeye tuna (*Thunnus obesus*) dive behavior in the central North Pacific Ocean. Prog. Oceanogr. 86:81–93.

Lehodey, P.
2001. The pelagic ecosystem of the tropical Pacific: dynamic spatial modelling and biological consequences of ENSO. Prog. Oceanogr. 49:439-468.

Lehodey, P., M. Bertignac, J. Hampton, A. Lewis, and J. Picaut.
1997. El Niño Southern Oscillation and tuna in the western Pacific. Nature 389:715–718.

Lehodey, P., F. Chai, and J. Hampton.
2003. Modelling climate-related variability of tuna populations from a coupled—ocean biogeochemical-populations dynamics model. Fish. Oceanogr. 12:483–494.

Lehodey, P., I. Senina, J. Sibert, L. Bopp, B. Calmettes, J. Hampton, and R. Murtugudde.
2010. Preliminary forecast of Pacific bigeye tuna population trends under the A2 IPCC scenario. Prog. Oceanogr. 86:302–315.

Marsac, F. and J. L. Blanc.
1999. Oceanographic changes during the 1997–1998 El Niño in the Indian Ocean and their impact on the purse seine fishery. IOTC Proceedings 2:147–157.

McPhaden, M. J.
1999. Genesis and evolution of the 1997–1998 El Niño. Science 283:950–954.

Miller, K. A.
2007. Climate variability and tropical tuna: management challenges for highly migratory fish stocks. Mar. Policy 31:56–70.

Miyake, M., P. Guillotreau, C-H. Sun, and G. Ishimura.
2010. Recent developments in the tuna industry: stocks, fisheries, management, processing, trade and markets. FAO Fisheries and Aquaculture Tech. Paper No. 543, 125 p.

Mohri M., and T. Nishida.
1999. Distribution of bigeye tuna (*Thunnus obesus*) and its relationship to the environmental conditions in the Indian Ocean based on the Japanese longline fisheries information. IOTC Proceedings 2:221–230.

Molcard, R., M. Fieux, and F. Syamsudin.
2001. The throughflow within Ombai Strait. Deep-Sea Res. (I Oceanogr. Res. Pap.) 48:1237–1253.

Murtugudde, R. G., S. R. Signorini, J. R. Christian, A. J. Busalacchi, C. R. McClain, and J. Picaut.
1999. Ocean color variability of the tropical Indo-Pacific basin observed by SeaWiFS during 1997–1998. J. Geophys. Res. (C Oceans) 104:18351–18366.

Otero, M. P, and D. A. Siegel.
2004. Spatial and temporal characteristics of sediment plumes and phytoplankton blooms in the Santa Barbara channel. Deep-Sea Res. (II Top. Stud. Oceanogr.) 51:1129–1149.

Pepperell, J.
2010. Fishes of the open ocean: a natural history and illustrated guide, 272 p. Univ. Chicago Press, Chicago.

Polacheck, T.
1991. Measures of effort in tuna longline fisheries: changes at the operational level. Fish. Res. 12:75–87.

Polovina, J. J., G. H. Balazs, E. A. Howell, D. M. Parker, M. P. Seki, and P.H. Dutton.
2004. Forage and migration habitat of loggerhead (*Caretta caretta*) and olive ridley (*Lepidochelys olivacea*) sea turtles in the central North Pacific Ocean. Fish. Oceanogr. 13:36–51.

Polovina, J. J., and E. A. Howell.
2005. Ecosystem indicators derived from satellite remotely sensed oceanographic data for the North Pacific. ICES J. Mar. Sci. 62:319–327.

Polovina, J. J., E. Howell, D. R. Kobayashi, and M. P. Seki.
2001. The transition zone chlorophyll front, a dynamic global feature defining migration and forage habitat for marine resources. Prog. Oceanogr. 49:469–483.

R Development Core Team.
2011. R: a language and environment for statistical

computing. R Foundation for Statistical Computing, Vienna, Austria. [Available from http://www.r-project.org, accessed February 2012.]

Radiarta, I. N., and S. Saitoh.
2008. Satellite-derived measurements of spatial and temporal chlorophyll-*a* variability in Funka Bay, southwestern Hokkaido, Japan. Estuar. Coast. Shelf Sci. 79:400–408.

Saitoh, S., E. Chassot, R. Dwivedi, A. Fonteneau, H. Kiyofuji, B. Kumari, M. Kuno, S. Matsumura, T. Platt, M. Raman, S. Sathyendranath, H. Solanki, and F. Takahashi.
2009. Remote sensing applications to fish harvesting. *In* Remote sensing in fisheries and aquaculture. Reports of the International Ocean-Colour Coordinating Group (IOCCG), No. 8 (M.-H. Forget, V. Stuart, and T. Platt, eds.), p.57–76. IOCCG, Dartmouth, Canada.

Song, L., and Y. Zhou.
2010. Developing an integrated habitat index for bigeye tuna (*Thunnus obesus*) in the Indian Ocean based on longline fisheries data. Fish. Res. 105:63–74.

Song, L., J. Zhou, Y. Zhou, T. Nishida, W. Jiang, and J. Wang.
2009. Environmental preferences of bigeye tuna, *Thunnus obesus*, in the Indian Ocean: an application to a longline fishery. Environ. Biol. Fishes 85:153–171.

Sprintall, J., J. C. Chong, F. Syamsudin, W. Morawit, S. Hautala, N. Bray, and S. E. Wijffels.
1999. Dynamics of the South Java Current in the Indo-Australian Basin. Geophys. Res. Lett. 26:2493–2496.

Sprintall, J., S. E. Wijffels, R. Molcard, and I. Jaya.
2009. Direct estimates of the Indonesian Throughflow entering the Indian Ocean: 2004–2006. J. Geophys. Res. (C Oceans) 114:1–19.
2010. Direct evidence of the South Java Current system in Ombai Strait. Dyn. Atmos. Oceans 50:140–156.

Syamsudin, F., A. Kaneko, and D. B. Haidvogel.
2004. Numerical and observational estimates of Indian Ocean Kelvin wave intrusion into Lombok Strait. Geophys. Res. Lett. 31:L24307. doi:10.1029/2004GL021227.

Teo, S. L. H, and B. A. Block.
2010. Comparative influence of ocean conditions on yellowfin and Atlantic bluefin tuna catch from longlines in the Gulf of Mexico. PLOS ONE 5(5):e10756. doi:10.1371/journal.pone.0010756.

Tolan, J. M, and M. Fisher.
2009. Biological response to changes in climate patterns: population increases of gray snapper (*Lutjanus griseus*) in Texas bays and estuaries. Fish. Bull. 107:36–44.

Torres-Orozco, E., A. Muhlia-Melo, A. Trasvina, and S. Ortega-Garcia.
2006. Variation in yellowfin tuna (*Thunnus albacares*) catches related to El Niño-Southern Oscillation events at the entrance to the Gulf of California. Fish. Bull. 104: 197–203.

Walters, C.
2003. Folly and fantasy in the analysis of spatial catch rate data. Can. J. Fish. Aquat. Sci. 60:1433–1436.

Ward, P.
2008. Empirical estimates of historical variations in the catchability and fishing power of pelagic longline fishing gear. Rev. Fish Biol. Fish. 18:409–426.

Ward, P., and R. A. Myers.
2004. Inferring the depth distribution of catchability for pelagic fishes and correcting for variations in the depth of longline fishing gear. Can. J. Fish Aquat.Sci. 62:1130–1142.

Wessel, P., and W. H. F. Smith.
1998. New, improved version of Generic Mapping Tools released. EOS Trans Am Geophys 79:579. [Available from http://gmt.soest.hawaii.edu, accessed February 2013.]

Wood, S. N.
2006. Generalized additive models: an introduction with R, 392 p. Chapman & Hall/CRC, Boca Raton, FL.

Yoder, J. A, and M. A. Kennely.
2003. Seasonal and ENSO variability in global ocean phytoplankton chlorophyll derived from 4 years of SeaWiFS measurements. Global Biogeochem. Cycles 17(4):1112. doi:10.1029/2002GB001942.

Zainuddin, M., S. Saitoh, and K. Saitoh.
2004. Detection of potential fishing ground for albacore tuna using synoptic measurements of ocean color and thermal remote sensing in the northwestern North Pacific. Geophys. Res. Lett. 31:L20311. doi:10.1029/2004GL021000.

Zhou, L., R. Murtugudde, and M. Jochum.
2008. Dynamics of the intraseasonal oscillations in the Indian Ocean South Equatorial Current. J. Phys. Oceanogr. 38:121–132.

Zuur, A. F., E. N. Ieno, N. J. Walker, A. A. Saveliev, and G. M. Smith.
2009. Mixed effects models and extensions in ecology with R, 574 p. Springer, New York.